Simultaneous Position, Velocity, Attitude, Angular Rates, and Surface Parameter Estimation Using Astrometric and Photometric Observations

Charles J. Wetterer and C. Channing Chow

Pacific Defense Solutions, LLC
Kihei, Hawaii, USA
jack.wetterer@pacificds.com

John L. Crassidis and Richard Linares

Department of Mechanical & Aerospace Engineering
University at Buffalo
Amherst, New York, USA
johnc@buffalo.edu

Moriba K. Jah

Air Force Research Laboratory, Space Vehicles Directorate
Kirtland AFB, New Mexico, USA
moriba.jah@kirtland.af.mil

Abstract—**Astrometric and photometric data fusion for the purposes of simultaneous position, velocity, attitude, and angular rate estimation has been demonstrated in the past. This state estimation is extended to include the various surface parameters associated with the bidirectional reflectance distribution function (BRDF). Additionally, a physically consistent BRDF and radiation pressure model is utilized thus enabling an accurate physical link between the observed photometric brightness and the attitudinal dynamics and ultimately the orbital dynamics. An example scenario is then presented where the model is an uncontrolled High Area to Mass Ratio (HAMR) object in geosynchronous Earth orbit and the position, velocity, attitude, angular rates, and surface parameters are estimated simultaneously**

Keywords—estimation; data fusion; BRDF

I.   INTRODUCTION

Wetterer and Jah [1] first demonstrated how brightness (photometric flux intensity) measurements can be used to estimate the attitude and angular rates of a space object (SO). Linares et al. [2] recently demonstrated a mechanism that fuses both angles (line-of-sight) and brightness measurements for the purpose of orbit, attitude, and shape determination. Whereas angles measurements are direct observations of the SO's orbital position, the brightness measurement is dependent on orbital position and the SO's shape, surface parameters and attitude, and thus provides an indirect observation of these other attributes. The physical correlation between the SO's shape/attitude and its orbital position are caused by the various non-gravitational forces and torques, such as radiation pressures that produce a linear and angular acceleration on the SO. These radiation pressures must be consistent with the surface bidirectional reflectance distribution functions (BRDFs), as shown by Wetterer et al. [3].

The work presented here expands the parameters that are included in the state to include those associated with the space object's surface, namely, the various BRDF parameters. First, the parameters included in the SO's "augmented" state are presented and the state function detailing the dynamics for each of these parameters in how they are propagated forward in time is defined. It is important to note that through radiation pressure, the BRDF parameters and other potential parameters in the augmented state influence the dynamics that affect both the attitude and orbit and thus influence the evolution of the system from point to point. As with the "classical" state parameters, these new parameters are intrinsic and unique properties of the system. Next, the unscented Kalman Filter (UKF) is briefly reviewed. Finally, test cases using an example scenario are examined in detail to demonstrate simultaneous estimation, effect of model mismatch, and information dilution.

II.   BUILDING THE AUGMENTED STATE

An Earth orbiting SO's attitude, angular rates, position, velocity, size, shape, mass and surface characteristics are all needed for high fidelity orbit propagation and in calculating associated measurements that are remotely observable, such as angles and brightness. All of these parameters make up the SO's "augmented" state. In this paper, we will include the SO's attitude, angular rates, position, velocity, and surface characteristics in the augmented state.

In this paper, the quaternion, which is based on the Euler angle/axis parameterization and contains four values, is used to specify the SO's attitude. The quaternion is defined as $\mathbf{q} = \begin{bmatrix} \boldsymbol{\xi} & q_4 \end{bmatrix}$ with $\boldsymbol{\xi} = \begin{bmatrix} q_1 & q_2 & q_3 \end{bmatrix} = \hat{\mathbf{e}}\sin(\upsilon/2)$ and

1. REPORT DATE **JUL 2013**	2. REPORT TYPE	3. DATES COVERED **00-00-2013 to 00-00-2013**

4. TITLE AND SUBTITLE **Simultaneous Position, Velocity, Attitude, Angular Rates, and Surface Parameter Estimation Using Astrometric and Photometric Observations**	5a. CONTRACT NUMBER
	5b. GRANT NUMBER
	5c. PROGRAM ELEMENT NUMBER
6. AUTHOR(S)	5d. PROJECT NUMBER
	5e. TASK NUMBER
	5f. WORK UNIT NUMBER

7. PERFORMING ORGANIZATION NAME(S) AND ADDRESS(ES) **Pacific Defense Solutions, LLC,1300 North Holopono Street Suite 116,Kihei,HI,96753**	8. PERFORMING ORGANIZATION REPORT NUMBER
9. SPONSORING/MONITORING AGENCY NAME(S) AND ADDRESS(ES)	10. SPONSOR/MONITOR'S ACRONYM(S)
	11. SPONSOR/MONITOR'S REPORT NUMBER(S)

12. DISTRIBUTION/AVAILABILITY STATEMENT **Approved for public release; distribution unlimited**

13. SUPPLEMENTARY NOTES **Presented at the 16th International Conference on Information Fusion held in Istanbul, Turkey on 9-12 July 2013. Sponsored in part by Office of Naval Research Global.**

14. ABSTRACT

Astrometric and photometric data fusion for the purposes of simultaneous position, velocity, attitude, and angular rate estimation has been demonstrated in the past. This state estimation is extended to include the various surface parameters associated with the bidirectional reflectance distribution function (BRDF). Additionally, a physically consistent BRDF and radiation pressure model is utilized thus enabling an accurate physical link between the observed photometric brightness and the attitudinal dynamics and ultimately the orbital dynamics. An example scenario is then presented where the model is an uncontrolled High Area to Mass Ratio (HAMR) object in geosynchronous Earth orbit and the position, velocity, attitude, angular rates, and surface parameters are estimated simultaneously.

15. SUBJECT TERMS

16. SECURITY CLASSIFICATION OF:			17. LIMITATION OF ABSTRACT	18. NUMBER OF PAGES	19a. NAME OF RESPONSIBLE PERSON
a. REPORT **unclassified**	b. ABSTRACT **unclassified**	c. THIS PAGE **unclassified**	**Same as Report (SAR)**	**8**	

$q_4 = \cos(\upsilon/2)$, where $\hat{\mathbf{e}}$ and υ are the Euler axis of rotation and rotation angle, respectively. In addition, each component's angular rate is denoted by $\omega = [\omega_x\ \omega_y\ \omega_z]$ as defined in the SO's body-fixed frame. A single position and velocity corresponding to the SO's center of mass, denoted by $r^I = [x\ y\ z]^I$ and $v^I = [v_x\ v_y\ v_z]^I$ respectively, are used, where the superscript I indicates the inertial frame. This is the classic 6DOF representation of the SO's orbit.

Each material that makes up the SO could reflect light differently. Thus, a SO might have many parameters that specify its surface properties. The function that defines how light is reflected from an opaque surface with a given surface normal direction ($\hat{\mathbf{N}}$), illumination direction ($\hat{\mathbf{L}}$ with angles θ_i and ϕ_i from $\hat{\mathbf{N}}$), and observer direction ($\hat{\mathbf{V}}$ with angles θ_r and ϕ_r from $\hat{\mathbf{N}}$) as shown in Fig. 1 is called the bidirectional reflectance distribution function (BRDF).
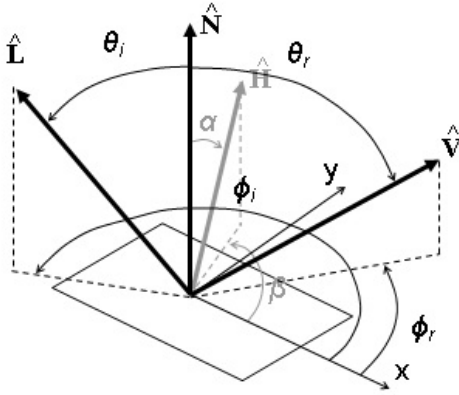

Fig. 1. The geometry of reflection

The BRDF is given by

$$f_r(\theta_i,\phi_i;\theta_r,\phi_r;\lambda) = \frac{dL_r(\theta_r,\phi_r)}{dE_i(\theta_i,\phi_i)} \quad (1)$$

where dL_r is the reflected radiance in $\mathrm{Wm^{-2}sr^{-1}}$ and dE_i is the irradiance in $\mathrm{Wm^{-2}}$. The bisector vector between the illumination source and the observer is

$$\hat{\mathbf{H}} = (\hat{\mathbf{L}}+\hat{\mathbf{V}})/|\hat{\mathbf{L}}+\hat{\mathbf{V}}| \quad (2)$$

with angles α and β from $\hat{\mathbf{N}}$ and is used in many analytic BRDF models.

There are many different reflectance models that could be used, but all can be expressed in a common nomenclature with the general BRDF calculated by

$$f_r = (dR_d + sR_s) \quad (3)$$

which depends on the diffuse bidirectional reflectance (R_d) and the specular bidirectional reflectance (R_s) and the fraction of

each to the total (d and s respectively where $d + s = 1$). These bidirectional reflectances are calculated differently for the various models. In this paper we will use the Ashikhmin-Shirley BRDF [4], also known as the Anisotropic Phong BRDF, where the diffuse and specular bidirectional reflectances are calculated using

$$R_d = \frac{28\rho}{23\pi}(1-sF_0)\left(1-\left(1-\frac{\hat{\mathbf{N}}\cdot\hat{\mathbf{L}}}{2}\right)^5\right)\left(1-\left(1-\frac{\hat{\mathbf{N}}\cdot\hat{\mathbf{V}}}{2}\right)^5\right) \quad (4)$$

$$R_s = \frac{\sqrt{(n_u+1)(n_v+1)}}{8\pi}\frac{F}{(\hat{\mathbf{V}}\cdot\hat{\mathbf{H}})\max[\hat{\mathbf{N}}\cdot\hat{\mathbf{L}},\hat{\mathbf{N}}\cdot\hat{\mathbf{V}}]}(\cos\alpha)^{n_u\cos^2\beta+n_v\sin^2\beta} \quad (5)$$

where (4) is a non-Lambertian diffuse BRDF, and the Fresnel reflectance (F) in (5) is given by Schlick's approximation [5]

$$F = F_0 + \left(\frac{1}{s}-F_0\right)(1-\hat{\mathbf{V}}\cdot\hat{\mathbf{H}})^5 \quad (6)$$

In addition to d, ρ and F_0, the Ashikhmin-Shirley BRDF has two exponential factors (n_u, n_v) that define the anisotropic reflectance properties of each surface. Without loss of functionality, the diffuse reflectance and the specular reflectance at normal incidence can be set equal to each other ($\rho = F_0$) and the difference between the diffuse and specular reflectances displayed in the diffuse fraction parameter, d. Additionally, for the sake of simplicity, in this paper the two exponential factors are set equal to each other as well ($n_u = n_v = n$). Thus, there are three unique surface parameters per surface (n, ρ, d). These surface parameters have constraints ($n > 0$, $0 \le \rho \le 1$, $0 \le d \le 1$). To account for the constraints within the filter, unconstrained proxy values are used in the state vector and estimation filter and these proxy values are converted back to the surface parameter value when needed. The conversion equations to the proxy value and from the proxy value for each of the surface parameters are

$$p_1 = \ln(n), \quad n = \exp(p_1) \quad (7)$$

$$p_2 = \frac{1}{2}\ln\left(\frac{\rho}{1-\rho}\right), \quad \rho = \frac{1}{2}(\tanh(p_2)+1) \quad (8)$$

$$p_3 = \frac{1}{2}\ln\left(\frac{d}{1-d}\right), \quad d = \frac{1}{2}(\tanh(p_3)+1) \quad (9)$$

The shape model will be built as the sum of facets where each facet has a position in the body frame and is specified by a particular area and normal vector. The SO's brightness is also calculated by summing the contribution to the brightness by each facet using the BRDF in the equation

$$m_{object} = m_{Sun} - 2.5\log_{10}\left(\frac{\sum\limits_{i=1}^{N_{facets}} A_i(f_r)_i\left(\hat{\mathbf{N}}_i \cdot \hat{\mathbf{L}}\right)\left(\hat{\mathbf{N}}_i \cdot \hat{\mathbf{V}}\right)}{r^2}\right) \quad (10)$$

where A_i is the area of the ith facet, r is the distance between the SO and observer, and m_{Sun} is the apparent magnitude of the illumination source (in this case the Sun).

So, in summary, the augmented state is

$$\hat{x} = \begin{bmatrix} \mathbf{q} & \boldsymbol{\omega} & \mathbf{r}^I & \mathbf{v}^I & \mathbf{p} \end{bmatrix}^T \quad (11)$$

where $\hat{x}$ is a 1×16 vector of real numbers and $\mathbf{p} = [p_1\ p_2\ p_3]$ is a vector containing the surface parameter proxy values.

III. PARAMETER PROPOGATION

The Newtonian two-body gravitational equations of motion with radiation pressure acceleration in Earth-centered inertial coordinates (ECI) are given by

$$\ddot{\mathbf{r}}^I = -\frac{\mu}{\|\mathbf{r}^I\|^3}\mathbf{r}^I + \mathbf{a}_{J2}^I + \mathbf{a}_{total}^I \quad (12)$$

where the terms μ represents the gravitational parameter of the Earth, $\mathbf{a}_{J2}^I$ is the gravitational perturbation due to non-symmetric distribution of mass along the lines of latitude, and $\mathbf{a}_{total}^I = \sum\limits_{i=1}^{N_{facets}} \mathbf{a}_i^I$ represents the acceleration perturbation due the various radiation pressures and summed over all the surfaces. Details regarding the calculation of this last term can be found in [3].

The attitude matrix for each component of the SO can be written as a function of the component's quaternion by

$$A = \Xi(\mathbf{q})^T \Psi(\mathbf{q}) \quad (13)$$

where

$$\Xi(\mathbf{q}) = \begin{bmatrix} q_4 I_{3\times3} + [\boldsymbol{\xi} \times] \\ -\boldsymbol{\xi}^T \end{bmatrix} \quad (14)$$

$$\Psi(\mathbf{q}) = \begin{bmatrix} q_4 I_{3\times3} - [\boldsymbol{\xi} \times] \\ -\boldsymbol{\xi}^T \end{bmatrix} \quad (15)$$

and

$$[\mathbf{a}\times] = \begin{bmatrix} 0 & -a_3 & a_2 \\ a_3 & 0 & -a_1 \\ -a_2 & a_1 & 0 \end{bmatrix} \quad (16)$$

is the skew-symmetric matrix representation of the cross product for any general 3×1 vector $\mathbf{a}$. The quaternion kinematics equation is given by

$$\dot{\mathbf{q}} = \frac{1}{2}\Xi(\mathbf{q})\boldsymbol{\omega} \quad (17)$$

where $\boldsymbol{\omega}$ is the component's angular velocity. The angular velocity dynamic equation can be written as

$$\dot{\boldsymbol{\omega}} = \bar{\bar{J}}^{-1}\left(\mathbf{M} - [\boldsymbol{\omega}\times]\bar{\bar{J}}\boldsymbol{\omega}\right) \quad (18)$$

where $\bar{\bar{J}}$ the inertia tensor for the SO and $\mathbf{M}$ are any external applied torques. The radiation pressure moments can be calculated by considering that the forces act through the center of each facet

$$\mathbf{M} = m \sum\limits_{i=1}^{N_{facets}} \left[\mathbf{r}_i^B \times\right] A(\mathbf{q})\mathbf{a}_i^I \quad (19)$$

where $\mathbf{r}_k^B$ is the location of the geometric center of each facet with respect to the center of mass of the SO in body coordinates and $A(\mathbf{q})$ is the attitude matrix calculated by the quaternion $\mathbf{q}$.

The surface properties are assumed to be constants, and so their dynamics equation can be written as

$$\dot{\mathbf{p}} = 0 \quad (20)$$

IV. UNSCENTED KALMAN FILTER

In this paper, the quaternion-based unscented Kalman filter (UKF) of Crassidis and Markley [6,7] is employed with the attitude state errors represented as error Generalized Rodrigues Parameters (GRPs) [8]. The augmented state is the SO's orientation and rotation rate, and the SO's position, velocity, and surface parameters given by (11).

The parameter propagation equations in (12), (17), (18), and (20) can be written in the general state function which gives the deterministic part of the stochastic model

$$\hat{x}_k^- = f\left(\hat{x}_{k-1}^+, w_k\right) \quad (21)$$

where w_k is the process noise vector

In this approach, the observation vector includes the apparent magnitude as computed with (10), as well as

astrometric measurements of the right ascension and declination of the SO:

$$\hat{y} = \begin{bmatrix} m_{object} & RA & Dec \end{bmatrix}^T \qquad (22)$$

where $\hat{y}$ is a 1×3 vector of real numbers. The general measurement function used in the estimation filter is:

$$\hat{y}_k = h\left(\hat{x}_k^-, v_k\right) \qquad (23)$$

where v_k is the measurement noise vector.

V. SIMULATIONS

The particular example will be that of simultaneously estimating the position, velocity, attitude, angular rates, and surface parameters of a HAMR object in geosynchronous Earth orbit (GEO). Table I lists the initial truth state, the initial estimated state, and the initial uncertainty.

The shape is defined as a cube with 1-m sides and a mass of 2 kg. Each surface of the cube is coated with the same BRDF surface parameters. The orbit was set to geosynchronous ($a = 42364.16932$ km, $e = 0$, $i = 30^o$, $M_0 = 91^o$, $\omega = 0$, $\Omega = 0$). Observations were simulated starting at 2010 Mar 15 at 4:00:00 UT, 1800 observations every 2 s (for a total of 1 hour), with an observation site corresponding to the top of Haleakala on Maui (latitude = 20.71 deg, longitude = -156.26 deg, altitude = 3.0586 km). The Thermal Radiation Pressure (TRP) parameters of each surface were $C = 9000$ J/K, $K = 25.5$ W/K, and $T_{body} = 243.5$ K. The measurement noise is 0.1 mag for the brightness observation and 10 arc-sec in the right ascension and declination observations.

TABLE I.   TESTS #1/#2 AUGMENTED STATE SETUP

Value in State	Initial Truth	Initial Estimate	Uncertainty
q	0.754	0.695	3.33 deg
	0.133	0.134	
	0.000	0.010	
	0.643	0.706	
ω (rad/s)	0.00200	0.00212	1.16×10^{-4}
	-0.00100	-0.00106	
	0.00500	0.00506	
r^I (km)	-739.4	-789.4	100
	36682.9	36732.9	
	21178.9	21278.9	
v^I (km/s)	-3.0669	-3.0169	0.10
	-0.0464	0.0536	
	-0.0268	-0.0768	
n	150	140	10
ρ	0.40	0.30	0.10
d	0.70	0.80	0.10

In the first two tests, the physically-consistent BRDF/Solar Radiation Pressure (SRP)/TRP model was used to generate the truth. In the first test, this same model was used in the state function of the UKF estimation while in the second test, a simplified SRP model (where the BRDF has a Lambertian diffuse component and a mirror-like specular component) and no TRP model was used in the state function. Figs. 2-4 plot the measurements over the observation period.

Figs. 5-7 plot selected components of the estimated state and covariance as a function of time for Test #1 while Figs. 8-10 plot the same for Test #2.
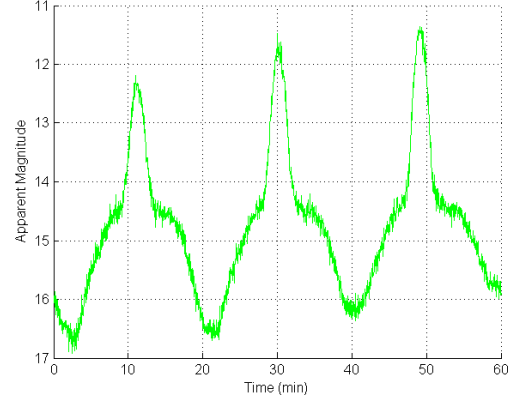
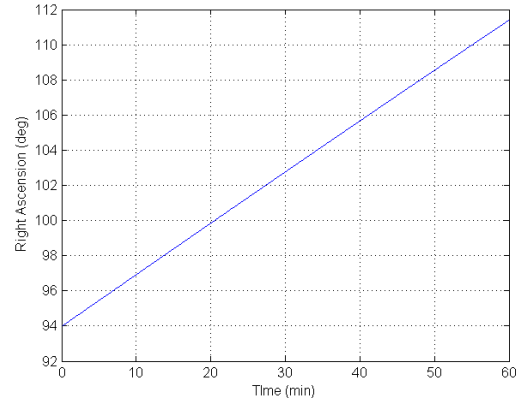

Fig. 2.   Brightness in magnitudes as function of time

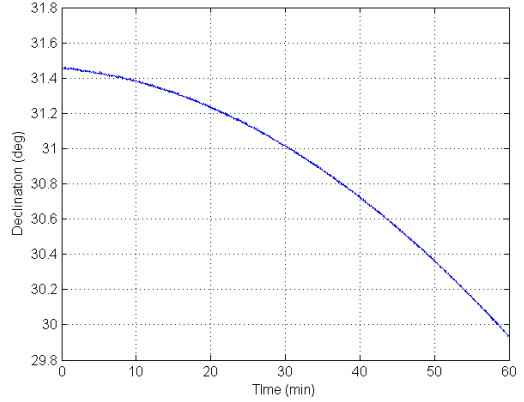Fig. 3.   Right Ascension as function of time
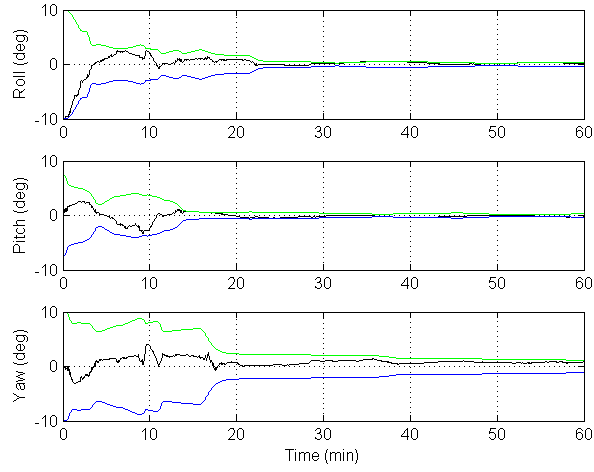

Fig. 4.   Declination as function of time

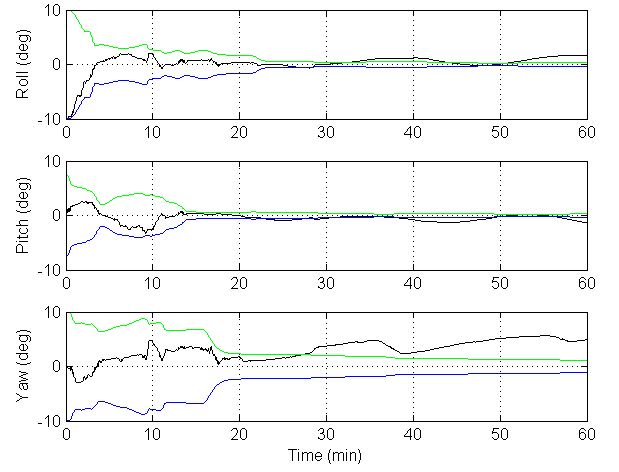Fig. 5. Attitude difference from truth and 3-σ error bounds for Test #1

Fig. 8. Attitude difference from truth and 3-σ error bounds for Test #2

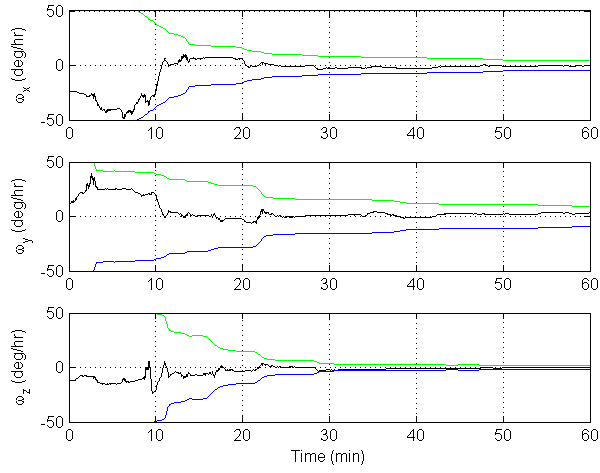

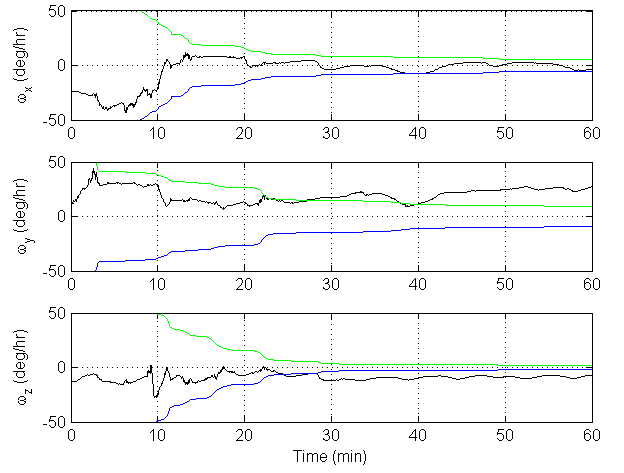Fig. 6. Angular rate difference from truth and 3-σ error bounds for Test #1

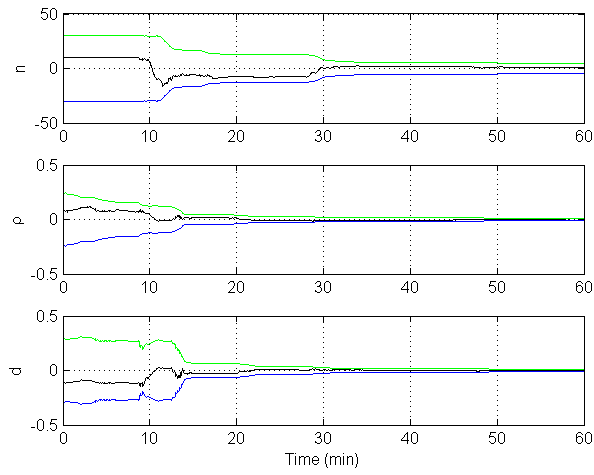Fig. 9. Angular rate difference from truth and 3-σ error bounds for Test #2

Fig. 7. Surface parameter difference from truth and 3-σ error bounds for Test #1
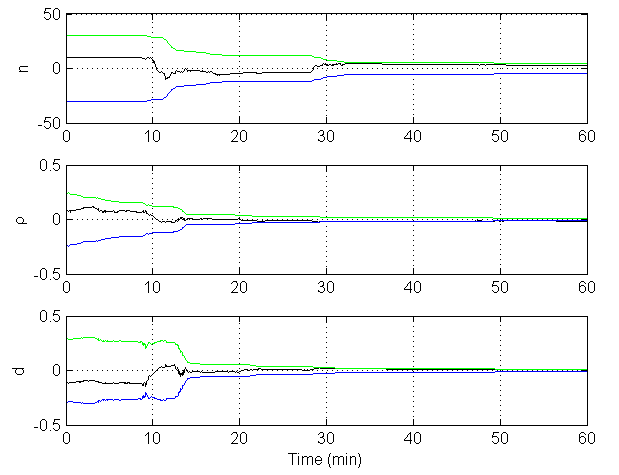

Fig. 10. Surface parameter difference from truth and 3-σ error bounds for Test #2

Value in State	Test #1		Test #2	
	Difference from Truth	*Uncertainty*	*Difference from Truth*	*Uncertainty*
Euler angle (deg)	0.152	0.131	1.628	0.126
	-0.267	0.106	-1.365	0.110
	0.828	0.391	4.898	0.376
ω (deg/hr)	-0.273	1.467	-3.288	1.762
	3.253	3.131	27.184	2.972
	-0.158	0.509	-6.898	0.547
$\mathbf{r}^I$ (km)	29.4	22.4	28.1	22.4
	-75.5	57.4	-72.1	57.4
	-46.6	35.5	-44.5	35.5
$\mathbf{v}^I$ (km/s)	0.00694	0.00524	0.00663	0.00524
	-0.00046	0.00043	-0.00045	0.00043
	-0.00033	0.00026	-0.00032	0.00027
n	0.775	1.493	2.796	1.462
ρ	-0.0053	0.0032	-0.0164	0.0035
d	-0.0015	0.0031	0.0076	0.0035

Table II lists the difference between the final estimated state and truth, and the 1-σ uncertainty as calculated by the final covariance matrix for both tests. The attitude quaternion difference has been converted to the equivalent roll/pitch/yaw Euler angle differences.

Of particular note in Test #1 is that all parameters in the state are observable by the filter and converge to the correct values (i.e. all parameters to within 3-σ of the quoted uncertainty). In Test #2, however, due to the dynamics model mismatch, some parameters in the state are not converging, and the differences from truth of the final state for these parameters are well outside 3-σ of the quoted uncertainty (e.g. attitude Euler angle components > 10-σ from truth). Some of the parameters are unaffected (e.g. position and velocity) by the model mismatch over the one hour time scale sampled, but would undoubtedly be affected over a longer time span.

In the next two tests, the same initial conditions with the physically-consistent BRDF/SRP/TRP used to both generate the truth and in the estimation filter as in Test #1 are duplicated except that the uncertainties on the surface parameters are increased by a factor of 3 from those shown in Table I. Additionally, in Test #4, the difference from the truth and the uncertainties of the orbital and attitudinal state parameters are decreased by a factor of 10.

Figs. 11-15 display how the increased initial covariance for the surface parameters results in filter divergence by plotting all the state parameter differences from truth and the 3-σ uncertainty as a function of time for Test #3. In this test, even the position and velocity begin to diverge. In contrast, when the orbital and attitudinal state parameter uncertainties are decreased and the estimation rerun, as in Test #4, the filter is able to converge (although outside the 3-σ bound), despite the increased surface parameter uncertainty as shown in Fig. 16.
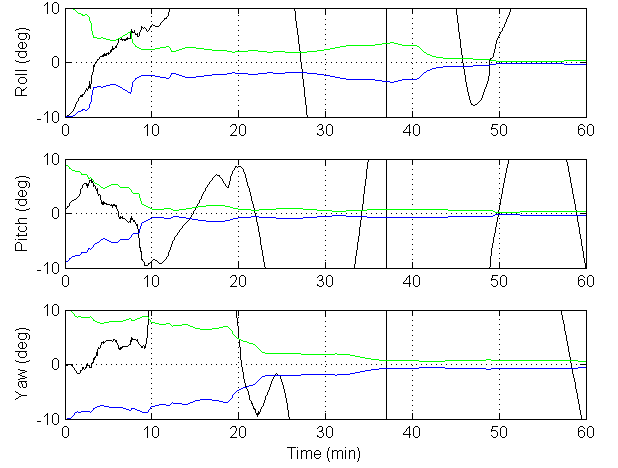
Fig. 11. Attitude difference from truth and 3-σ error bounds for Test #3
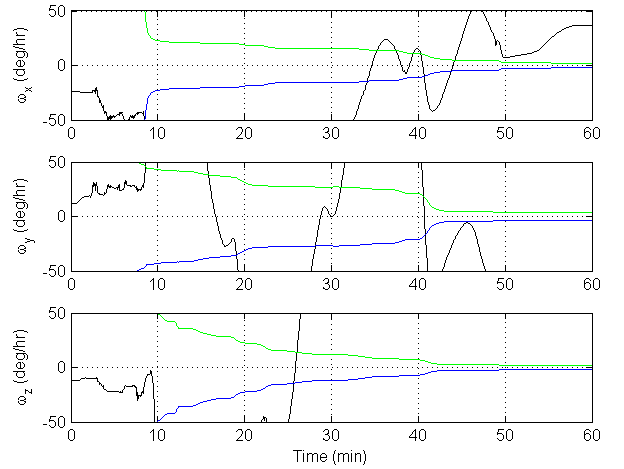
Fig. 12. Angular rates difference from truth and 3-σ error bounds for Test #3
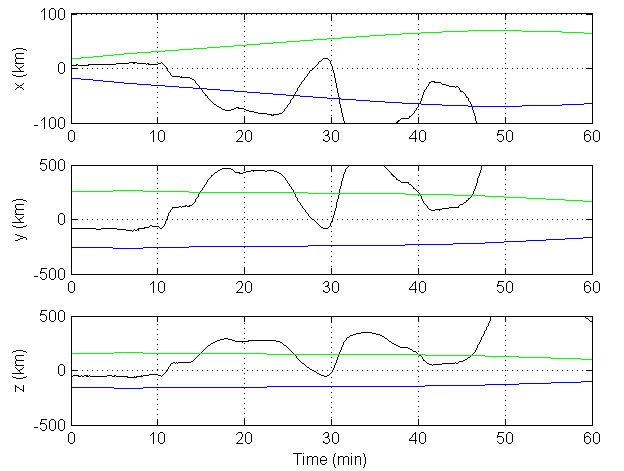
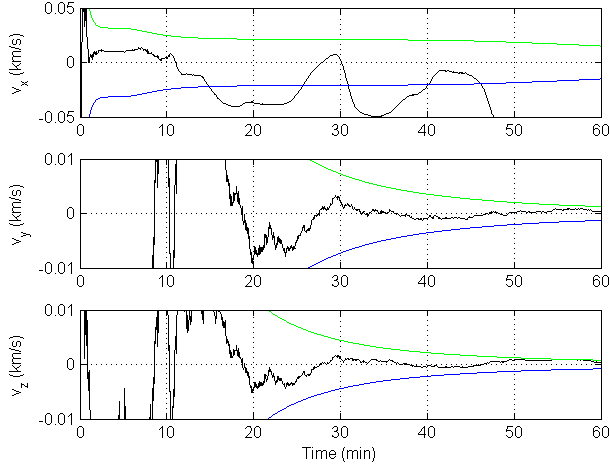Fig. 13. Position difference from truth and 3-σ error bounds for Test #3

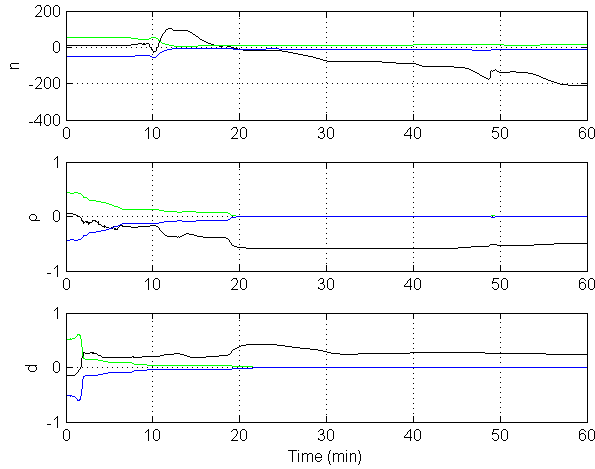Fig. 14. Velocity difference from truth and 3-σ error bounds for Test #3

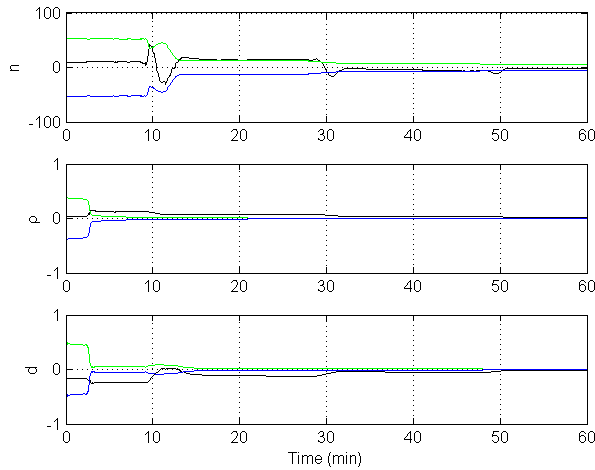Fig. 15. Surface parameter difference from truth and 3-σ error bounds for Test #3

Fig. 16. Surface parameter difference from truth and 3-σ error bounds for Test #4

Value in State	Test #3		Test #4	
	Difference from Truth	*Uncertainty*	*Difference from Truth*	*Uncertainty*
Euler angle (deg)	40.730	0.119	-0.457	0.119
	-10.058	0.130	-0.357	0.100
	-14.387	0.194	0.728	0.248
ω (deg/hr)	36.226	0.592	-1.506	0.918
	-112.338	1.087	3.807	1.599
	434.556	0.545	-1.151	0.413
$\mathbf{r}^I$ (km)	-279.5	21.5	-3.5	9.4
	715.9	54.9	8.9	24.0
	442.6	34.0	5.5	14.8
$\mathbf{v}^I$ (km/s)	-0.06546	0.00503	-0.00078	0.00220
	-0.00033	0.00043	-0.00035	0.00043
	-0.00040	0.00027	-0.00023	0.00027
n	-208.2	4.738	-2.666	1.630
ρ	-0.4960	0.0027	0.0248	0.0017
d	0.2388	0.0010	-0.0243	0.0023

Table III lists the difference between the final estimated state and truth, and the 1-σ uncertainty as calculated by the final covariance matrix for Test #3 and Test #4. The attitude quaternion difference has again been converted to the equivalent roll/pitch/yaw Euler angle differences. In Test #3, the filter is suffering from information dilution. There are simply too many parameters in the state whose uncertainties are large. When, however, as in Test #4 the uncertainties for only a limited number of state parameters are large, the filter is able to converge to close to the truth.

VI. CONCLUSIONS

Physically consistent BRDF, SRP, and TRP modeling enables astrometric and photometric data fusion for the purposes of simultaneously estimating orbital, attitudinal, and surface parameters of a space object. Other parameters associated with the space object, such as the mass and shape, could also be added to the augmented state vector and estimated provided that their effect on the system is observable with an appropriate measurement model. Caution is warranted, however, concerning model mismatches (both in the dynamics and the BRDF model) and the possibility of information dilution when too many quantities with large uncertainties are estimated at once.

REFERENCES

[1] Wetterer, C. J. & Jah, M. K., "Attitude estimation from light curves," *Journal of Guidance, Control, and Dynamics* 32: 1648-1651, 2009.

[2] Linares, R., Crassidis, J. L., Jah, M. K., and Kim, H., "Astrometric and Photometric Data Fusion for Resident Space Object Orbit, Attitude, and Shape Determination Via Multiple-Model Adaptive Estimation," *AAS/AIAA Astrodynamics Specialists Conference*, Vol. AIAA-8341, 2010.

[3] Wetterer, C. J., Linares, R., Crassidis, J. L., Kelecy, T. M., Ziebart, M. K., Jah, M. K., and Cefola, P. J., "Refining Space Object Radiation Pressure Modeling with Bidirectional Reflectance Distribution Functions," Proceedings of the AAS/AIAA Spaceflight Mechanics Conference, Kauai, HI, February 2013

[4] Ashikhmin, M., and Shirley, P., "An Anisotropic Phong BRDF Model," *Journal of Graphics Tools,* Vol. 5, No. 2, pp.25-32, 2000.

[5] Schlick, C., "An inexpensive BRDF model for physically-based rendering," *Computer Graphics Forum*, 13(3), pp. 233-246, 1994.

[6] Julier, S. J., Uhlmann, J. K., and Durrant-Whyte, H. F., "A New Approach for Filtering Nonlinear Systems," Proceedings of the American Control Conference, Seattle, WA, 1628–1632, June 1995.

[7] Crassidis, J. L. and Markley, F. L., "Unscented Filtering for Spacecraft Attitude Estimation," *Journal of Guidance, Control and Dynamics* 26, 536–542, 2003.

[8] Schaub, H. and Junkins, J. L., "Stereographic Orientation Parameters for Attitude Dynamics: A Generalization of the Rodrigues Parameters," *Journal of the Astronautical Sciences* 44, 1–20, 1996.